Contents lists available at ScienceDirect

Materials Today Bio

Degradable carrier-free spray hydrogel based on self-assembly of natural small molecule for prevention of postoperative adhesion

Linjun Zou [a], Yong Hou [a], Jiawen Zhang [a], Meiying Chen [a], Peiying Wu [b], Changcun Feng [b], Qinglong Li [a], Xudong Xu [a], Zhaocui Sun [a,*], Guoxu Ma [a,*]

[a] *Key Laboratory of Bioactive Substances and Resource Utilization of Chinese Herbal Medicine, Ministry of Education; Institute of Medicinal Plant Development, Peking Union Medical College and Chinese Academy of Medical Sciences, Beijing, 100193, China*
[b] *School of Pharmacy; Guangxi Medical University, Nanning, 530021, China*

ARTICLE INFO

ABSTRACT

Postoperative peritoneal adhesion (PPA) is frequent and extremely dangerous complication after surgery. Different tactics have been developed to reduce it. However, creating a postoperative adhesion method that is multifunctional, biodegradable, biocompatible, low-toxic but highly effective, and therapeutically applicable is still a challenge. Herein, we have prepared a degradable spray glycyrrhetinic acid hydrogel (GAG) based on natural glycyrrhetinic acid (GA) by straightforward heating and cooling without the use of any additional chemical cross-linking agents to prevent postoperative adhesion. The resultant hydrogel was demonstrated to possess various superior anti-inflammatory activity, and multiple functions, such as excellent degradability and biocompatibility. Specifically, spraying characteristic and excellent antibacterial activities essentially eliminated secondary infections during the administration of drugs in surgical wounds. In the rat models, the carrier-free spray GAG could not only slow-release GA to inhibit inflammatory response, but also serve as physical anti-adhesion barrier to reduce collagen deposition and fibrosis. The sprayed GAG would shed a new light on the prevention of postoperative adhesion and broaden the application of the hydrogels based on natural products in biomedical fields.

1. Introduction

Postoperative peritoneal adhesions (PPA) are one of the more universal complications of abdominal surgery caused by the pathological association between surgical trauma and nearby organs or tissues [1,2]. Following clinical surgery, the incidence rate can reach 90%with more than 40% resulting in adhesive intestinal obstruction. It also has the potential to cause complex syndromes, chronic abdominal pain, female infertility, organ dysfunction, and even death. Furthermore, in the United States alone, the treatment of peritoneal adhesion development costs up to $1.3 billion each year. In certain European nations, the direct medical expenditures for adhesion-related disorders exceeded the surgical costs for stomach cancer and were nearly as high as those for rectal cancer [3–5]. Given the enormity of the health issues and financial cost associated with adhesions, prevention of PPA have become urgently solved issue in the clinical field.

Current therapeutic measures for PPA include surgery [6], anti-adhesion drug [7], and barrier material [8,9], but their

effectiveness were not satisfactory [10,11]. Despite the fast advancement of minimally invasive surgery technologies, the advent of laparoscopy and the tactful handling of medical professionals can lessen the prevalence of PPA. They still cannot completely prevent their occurrence, and the recovery of secondary surgery may cause new adhesions more seriously [12,13]. As we all know, coagulation, inflammation and fibrinolysis that occur during tissue healing have a significant influence on the creation of adhesions [14–17]. Therefore, numerous medications that affect coagulation, inflammation, fibrinolysis, and associated cytokines have been utilized [18,19]. However, huge side effects, short duration of action and low therapeutic effect make people disappointed with drug treatment. For the existing physical barrier, it works by isolating the wound from peripheral tissue, thereby blocking the formation of fibrin bridges to prevent the formation of intra-abdominal adhesions [20–23]. Icodextrin 4% solution (Deerfield, Illinois, USA), Interceed® (Johnson &Johnson, Cincinnati, USA), Seprafilm® (Genzyme, Cambridge, USA), and other anti-adhesion materials have achieved certain curative effects, but there are a large number of

---

* Corresponding authors.
  E-mail addresses: flydancingsun@163.com (Z. Sun), mgxfl8785@163.com (G. Ma).

deficiencies, such as cumbersome synthesis process, high purchase cost, immunogenicity, lacking target coverage, lacking sustained release, and non-absorbability [23–27]. Recent advancements in the field of hydrogel have led to a renewed interest in physical barrier and eliminated most of the issues [27]. In order to meet the key period for adhesion formation (3–5 days following surgery), most hydrogels are formed by chemical cross-linking or physical adsorption of macromolecules with low biocompatibility. This makes clinical researchers and pharmacologists worry that foreign materials, particularly those from non-degradable components as implanted materials, may further lengthen the inflammatory response and thereby encourage PPA development [28,29]. Bacteria-related intraperitoneal infections may also promote the formation of PPA through activating and boosting the EGFR signaling in peritoneal mesothelial cells [5]. Therefore, the issue of subsequent wound infection should be taken into account while using physical isolation materials [30]. How to increase the anti-adhesion efficacy and reduce toxicity on the clinical prevention and intervention of PPA is worth of further exploration deeply.

Natural products originated from traditional Chinese medicine (TCM) are currently attracting significant research interest for prevention and treatment of human illnesses due to their inherent benefits, encompassing excellent biological activity, biocompatibility, degradability [31]. Numerous supramolecular hydrogels loading naturally occurring substances have been successfully prepared and used for inflammation relief [32], wound repair [33], bacterial resistance [34], and tumor inhibition [35,36]. However, it was constantly found that the most of hydrogel carriers might result in limited loading efficacy, poor biocompatibility and biodegradability, and potential adverse consequences [37]. To tackle these problems and lower the risks of novel material research, "self-delivery strategies" have been widely used to increase the bioavailability of active compounds in decades [38]. Generally, various supramolecular systems without structural modifications by the spontaneous self-assembly of bioactive natural small molecules are predicted to exhibit traits of improved therapeutic effectiveness, softer release, and reduced cytotoxicity [39]. Gallic acid self-assembled into a novel hydrogel, which Huang et al. discovered, might hasten the healing of wounds [39]. Moreover, it was demonstrated that the self-assembled betulinic acid had stronger anti-leukemic effects on the KG-1A and K562 cell lines [40]. In spite of several efforts, designing self-assembled hydrogels based on natural active molecules to prevent PPA remains a gap [12,41]. It is clearly evident that the small molecule with anti-adhesion therapy and physical barrier potential has not been discovered. The search for safer and more potent anti-PPA materials must continue.

As a natural bioactive compound from *Glycyrrhiza uralensis* Fisch. [42], GA had been proven to display extensive remarkable biological activities [43,44], including anti-inflammation [45], antibiosis [46], and anti-tumor [47]. Despite reports that GA may form gels in a range of organic solvents and NaOH [48,49]. However, unavoidable cytotoxicity induced by high gel concentration, the use of organic solvents and strong alkalinity might be extremely harmful to human body, which severely limited the biomedical application of GA. How to perfectly utilize the bioactivities and the gel properties of GA for prevention of PPA required further research. Fortunately, we have reported that a sprayed, hypo-basic, low-toxic and biodegradable hydrogel was prepared successfully based on GA and sodium carbonate solution by straightforward mixing and heating. Especially, it had provided a subversive strategy to reduce intraperitoneal bacterial infections and precisely meet the individual wound size. Results from *in vivo* and *vitro* tests showed that the GAG possessed good anti-inflammatory, antibacterial and anti-adhesion capacity. More importantly, its degradation cycle was in line with our requirements for the stability of anti-adhesion materials. The GAG could act as not only an adjunctive therapeutic drug to reduce inflammation and bacterial infection, but also a physical barrier to prevent and treat intestinal adhesions. To our best knowledge, there are still few reports of the intended natural hydrogel containing this sprayed self-delivery and physical isolation capability. It could circumvent expensive and time-consuming procedures for medicines and physical barriers, which had promising potential as an intestinal adhesion prevention material.

2. Materials and methods

2.1. Materials, cell lines, and animals

In this investigation, Glycyrrhetinic acid was acquired from Shanghai Aladdin Holdings Group Co., Ltd. Beijing Chemical Works, Beijing, China, provided all of the solvents used in this study, and the water was ultrapure grade. Male Kunming mice (18−22 g) and Sprague-Dawley (SD) rats (220−250 g) were acquired from SBF (Beijing) experimental animal Technology Co. Ltd. The experiments were carried out by the Institute of Medicinal Plant Development affiliated to the Chinese Academy of Medical Sciences (Beijing, China, Ethical review No. SLXD-20211225002).

2.2. Preparation of the GAG

GA was dissolved in a sodium carbonate solution, and then the mixture was homogenized using ultrasonic and stirring. The mixture was then heated at 70 °C for approximately 5 min. After cooling for 10 min, a homogeneous, stable gel was produced. the test tube tilt method and the test tube inversion method was used to confirm the formed GAG. The critical gel concentration (CGC) was then determined to be 28 mg/mL by control independent variable method. In general, firstly, in 1 mL of sodium carbonate solution (volume: 1 mL, the concentration: from 0.05 mol/L to 0.3 mol/L), the addition amount of GA was fixed at 20 mg. When sodium carbonate solution (1 mL, 0.05 mol/L) was used, a flowing opaque liquid was obtained. Then, when sodium carbonate solution (1 mL, 0.075 mol/L) was used, a stable gel was obtained. However, as the sodium carbonate (1 mL, 0.3 mol/L) was used in the formation of GAG, a flowing opaque liquid was obtained again. This phenomenon meant, when the amount of GA was 20 mg, the sodium carbonate solution (0.075 mol/L, 1 mL) was the minimum requirement for form GAG. Then, sodium carbonate solution (0.075 mol/L, 1 mL) was fixed quantity in the formation of GAG and the addition amount of GA (from 15 mg to 29 mg) was changed. In sodium carbonate solution (0.075 mol/L, 1 mL), when the amount of GA was less than 19 mg, the GAG gel could not be formed stably. On the contrary, in sodium carbonate solution (0.075 mol/L, 1 mL), when the addition amount of GA was 19 mg, a stable gel was again obtained. Unfortunately, when the addition amount of GA was more than 28 mg, the resulted solution became cloudy after heating. In addition, GA was practically insoluble in water [50]. These phenomena all indicated that there were GA molecules that did not form a gel in the solvent. Based on this phenomenon, it was determined that the optimal condition for GAG formation was determined as follow: sodium carbonate solution (0.075 mol/L) and GA (28 mg). Freeze-drying was used to produce the dried GAG.

2.3. Microscope and self-assembled mechanism study of the GAG

With the aid of Field-emission scanning electron microscope (JSM-6700F, JEOL, Japan), FEI Talos F200X instrument and a Bruker Dension Icon (Bruker AXS), SEM images, the corresponding elemental mapping images, TEM pictures and AFM images were captured. FT-IR (Nicolet IS10 instrument, Thermo, USA) and the NMR experiments (Bruker AV 600 NMR spectrometer, Bruker, USA) was used to explore self-assembled mechanism. A Zeta-sizer Nano ZS particle analyzer (Malvern Instrument Ltd) was used to calculate the surface charge. Circular dichroism (CD, J-1500, JASCO, Tokyo, Japan) analysis was used to look at the secondary structure.

2.4. Rheological experiments

Rheolaser MASTER™ (Formulaction, France) was used to record the gel development and collapse process. For measuring gel formation process, Glycyrrhetinic acid added to sodium carbonate solution. Then, GAG solution (clear GAG-sol) after heating in 70 °C water bath was placed in the instrument to be tested promptly at 25 °C. Subsequently, by increasing the temperature in the rheolaser by 1 °C per minute to 70 °C till GAG-sol was formed, the GAG collapse process was seen. The device would compute and output the pertinent data automatically.

2.5. Antimicrobial activity measurements

Gram-positive *S. aureus* and Gram-negative *E. coli* were cultivated in nutrient broth at 200 rpm in a rotary shaker overnight at 37 °C. Then they were adjusted in well with nutrient broth at a density of 2×10^6 CFU/mL. The GAG was serially incubated for 16 h at final concentrations ranging from 100 to 400 μg/mL (100, 150, 200, 300, 400 μg/mL). the bacterial suspension (100 μL) was put equally to each well. Nutrient broth was used as the solvent control. Then the cultured bacterial suspension was diluted 1×10^5 times (100 μL) and evenly coated on agar plates. The colonies produced were enumerated and compared to control plates after an 18-h incubation period at 37 °C to determine the inhibition rate.

Inhibition rate (%) = (counts of control − counts of samples)/counts of control × 100%. The parallel experiments were performed for three times [51].

2.6. In vitro biocompatibility of the GAG

The biocompatibility of GAG was assessed by MTT assay and hemolysis assay. H9c2 cells were seeded in 96-well plates at 1×10^5 cell mL^{-1}, 100 μL per well, and treated with GAG at different concentrations for 24 h. Then, MTT (5 mg/mL) was added to 96-well plates, 10 μL per well, and placed in cell culture incubator at 37 °C for 4 h. Following the removal of the supernatants, 150 μL of DMSO was added to each well to dissolve the formazan crystals. A microplate reader was used to measure the color intensity at 570 nm. Three times the parallel experiments were conducted. While calculating the relative cell activity for each experimental group, the absorbance value for the blank control group was 100%.

1 mL of mouse blood was centrifuged three times at 1500 rpm for 15 min each after being diluted with 0.9% NaCl, until obtained erythrocytes. Erythrocytes were reconstituted in 0.9% NaCl and combined with either a GAG sample, an ultrapure water group, or a normal saline group. The mixture was then incubated for 3 h at 37 °C in a water bath before the supernatant was collected. A microplate reader was used to measure the supernatant's absorbance at 570 nm. The following is the formula for calculating hemolytic percentage (HD):

HD (%) = $(A_s - A_n)/(A_p - A_n) \times 100\%$, Where, the absorbance values for the sample, the negative control, and the positive control were denoted as As, An, and Ap, respectively. There was no hemolysis when HD was less than 5%.

2.7. Spray-on setup

A simple and practical device was built to simulate the methods reported in the literature. Spray vials containing GAG gel and red pigment are placed before being sprayed at a predetermined distance. Press the spray bottle to its lowest pressure with each press to guarantee that the amount of each shot is as uniform as possible. Then, a 3D surface map was created using Image-J to illustrate the strength of the spray patterns [52].

2.8. In vitro release behavior studies

The *in vitro* release behavior of GAG in different temperature (room temperature and 37.8 °C) was detected by analysis of the weight of the residue. Initially, 1 mL of GAG sample was put to a dialysis bag (MWCO 3500 Da) and they are weighed. Then, the dialysis bag was added into 200 mL of PBS solution. At different time intervals (0, 1, 2, 3, 4, 5, 6, 7 day), the dialysis bag was removed and weighed. The loss weight was considered to be amount of GAG disintegration. At the same time, 5 mL of solution was taken out to calculate GA concentration in solution, and replaced with of 5 mL fresh PBS solution. The cumulative degradation ratio at various time was computed by measuring the mass of the remaining GAG. the release behavior and GA concentration of the GAG in 5 mL solution was respectively analyzed by HPLC and the concentration was calculated according to the standard curve. Three determinations were made to verify accuracy.

2.9. In vitro anti-inflammatory test and the ear edema test

The RAW264.7 cells were treated with different concentrations (6.25, 12.5, 25, 50, 100, 200uM) of GAG for 24 h, the viability of RAW264.7 cells was detected by MTT method and the effect of GAG on RAW264.7 cells was screened active safe dose range. ELISA: RAW264.7 cells were randomly divided into positive group (Indometacin), model group, control group, and GAG group. Model group: cells were stimulated with 500 ng/mL LPS; GAG group: GAG at a concentration in a safe dose range was added first, and then 500 ng/mL LPS was added to stimulate cells. Positive group: Indometacin was used as a positive control. Control: PBS was used as a control group. After reaching a certain drug action time, the culture was stopped and the supernatant was collected, and the level of inflammatory factor TNF-α was detected by enzyme-linked immunosorbent assay (ELISA) (Beijing Jiachen Technology Co., Ltd. Beijing, China).

Xylene-induced ear edema in the mouse model was carried out as described by Liu et al. [45]. Three groups of mice (n = 10) were created: control, GAG (28 mg/mL), and model and the control group was provided with water (0.1 mL each). Spraying therapy was applied to all groups for a total of seven days. After the last dosage, the left ears' front and rear surfaces were equally covered with xylene (0.02 mL), and the right ears were cleaned with normal saline (as control). The mice were euthanized after 30 min, and both ears were immediately removed. An 8-mm perforator was used to sample a portion of each ear, which was subsequently weighed. The following formula was used to determine the level of ear edema:

Ear edema degree = weight of the left ear − weight of the right ear

Following the collection of ear tissue samples, 10% formaldehyde fixation, paraffin embedding and H&E staining are performed. An electron microscope was used to view the histological alterations [53]. After homogenizing the ear tissues, the homogenates were centrifuged as previously mentioned [54]. The supernatants were gathered to check for TNF-α and PEG2 levels in accordance with the instructions of the ELISA kit (Beijing Jiachen Technology Co., Ltd. Beijing, China).

2.10. Adhesion of the GAG on a solid surface

The sliding and adhesion process was recorded by digital photos from an inclined view of about 30° and a side view. Initially, the fresh porcine small intestine is placed horizontally on the foam board, equipped with a suitable scale and then placed at an angle of 30°. 0.2 mL GAG droplet was sprayed on the initial scale. Under the same environmental conditions, the time it takes for the GAG to reach a fixed position (2, 5, 7 cm) is recorded. The time varying film formation behavior of the sprayed GAG was recorded with digital photos. Triplicates of each experiment were run.

2.11. In vivo antiadhesion evaluation

The *in vivo* antiadhesion effect of GAG was assessed in a rat side wall defect–cecum abrasion model. First, pentobarbital sodium was used to anesthetize the SD rats. Three alternate betadine and 75% ethanol scrubbing were used to prepare the abdomen skin. The abdominal wall was then cut along the midline with a single 4–5 cm-long incision using surgical scissors. The cecum was separated, and the serosal surface was gently rubbed with sterile surgical cotton until spotted bleeding emerged. A scalpel was used to create a 2 cm by 2 cm peritoneal defect on the corresponding side of the abdominal wall. In the GAG group, the GAG (1 mL) was sprayed over the cecum and damaged belly wall. In the negative control group, sterile saline (1 mL) was sprayed on the surface of a wound. 1 mL commercial hyaluronic acid (HA) hydrogel was as a positive control group. 14 SD rats are split among each group. To access the peritoneum and assess the adhesion, seven rats from each group were euthanized 7 and 14 days later. The adhesion that developed between the cecum and the abdominal wall was documented and scored using a common scoring system. The tissues from the cecum and abdominal wall that were affected by the damage and adhesion were then gathered and subjected to H&E and MT staining procedures for analysis.

2.12. Statistical analysis

All data were represented as mean ± SD (n = 3 to 7). Statistical analysis was calculated with an unpaired two-tailed Student's *t*-test or one-way analysis of variance (ANOVA) with Tukey's multiple comparison test using GraphPad Prism v.8.0 (GraphPad Software). *P < 0.05, **P < 0.01, ***P < 0.001, and ****P < 0.0001 were considered statistically significant.

3. Results and discussion

3.1. Preparation and characterization of GAG

The preparation of a hydrogel depends on the GA's ability to self-assemble. For the first time, we surprisingly observed that lower concentrations of sodium carbonate solution could easily promote the self-assembly of GA. A stable and opaque white GAG was gradually created by combining the desired quantity of GA powder with a solution of sodium carbonate after merely heating to 70 °C and cooling to room temperature. Then, the relationship between the concentration of sodium carbonate solution and the addition amount of GA to form GAG was further study by control independent variable method (Fig. S1 and S2). By changing the concentration of sodium carbonate solution and the addition amount of GA, the optimal condition for GAG formation was determined as follow: sodium carbonate solution (0.075 mol/L) and GA (28 mg). In this optimal condition, GA (28 mg) happened to be all involved in the formation of GAG in sodium carbonate solution (0.075 mol/L, 1 mL). Next, we tested the pH of the resulting GAGs formed by these different concentrations of GA. In general, the pH of the gel formed gradually decreased as the amount of GA added increased (Fig. S3). This result also corresponds to the fact that GA is a weakly acidic natural triterpenoid molecule reported in the literature [55]. Furthermore, the result showed that, in 0.075 mol/L sodium carbonate solution, the pH of the formed gel was almost unchanged when the dosage of GA exceeded 28 mg. For GAG prepared under the same sodium carbonate conditions, the addition amount of GA had little effect on cytotoxicity and did not make obvious toxicity to H9c2 cell (Fig. S4). Ho wever, reducing the alkalinity of GAG might make it more applicable for medical applications [56]. Thus, taking into account whether the influence of low pH or the optimal condition for GAG formation, the hydrogel formed by mixing 28 mg of GA with a sodium carbonate solution (0.075 mol/L, 1 mL) should be further investigated in this experiment.

Due to the different gel formation methods reported in the previous literature, Scanning Electron Microscopy (SEM), Transmission Electron Microscope (TEM) and Atomic Force Microscopy (AFM) were used to analyze the size and morphology of the final dried GAG. SEM images showed that nanofibers of different thicknesses extend to form entangled rope structures (Fig. 1A and Fig. S5). Furthermore, the data in corresponding elemental mapping images illustrated that Na, O and C elements were uniformly dispersed in GAG systems (Fig. 1B). The surface of GAG nanofibers was found to be relatively rough and multi-branched, and the closely entangled rope-like self-assembled structure also was displayed in TEM images (Fig. 1C and Fig. S6). As observed in AFM images, The rough and uneven surface structure further confirms that the GAG molecules aggregate to form cross-linked entangled structures (Fig. 1D and Fig. S7). As shown in Fig. 1E, the results from circular dichroism (CD) showed that the positive peak (right-hand helical arrangement) of GAG at 223 nm was weaker comparing with GA group, indicating there were differences in the chiral packing and the molecular packing of GA was slightly changed in the self-assembly process, which could be demonstrated through TEM (Fig. S8). Furthermore, it was discovered that GA power had a slightly negative surface charge that was closely related to the carboxyl group and hydroxyl group by measuring a negative zeta potential of −35.8 mV (Fig. 2F). In GAG, the GAG tended to aggregate to entangled rope-like self-assembled structure by intermolecular forces, which made the absolute value of zeta potential reduce to −4.63 mV. Together, these studies demonstrated that the GAG was successfully formed. In directly self-assembled mechanism study, the Fourier transform infrared (FT-IR) experiment demonstrated that the absorption peak of 30-carboxylate group was shifted from the 1705 cm^{-1} of free powder to 1556 cm^{-1} after gelation (Fig. S9). In comparison with the O–H stretching frequency of hydroxy group in the GA powder at 3439 cm^{-1}, the O–H stretching frequency of hydroxy group in dried GAG appeared at 3425 cm^{-1} accompanied by a decreased intensity and the absorption peak becomes broadened from a sharp peak which was considered as a hallmark of hydrogen bonding. Overall, these cases support the view that the driving forces for GAG were the hydrogen bonding, electrostatic interaction and dipole–dipole interaction, which are similar to those reported in the literature [49]. But we also discovered that, in the ^{1}H NMR spectrum, hydrogen signal peak at H-12 of GAG had changed and moved to higher field with the increase of GAG concentration (from 1 mg/mL to 10 mg/mL) (Fig. 1G). It was a proof of π-π interaction supported the self-assembly of GAG [57]. Based on these results, it was proposed that several GA molecules are stacked one by one to form fine fiber structure architecture by π-π interaction, hydrogen bonding and dipole–dipole interaction. Then, the macromolecules tend to bind tightly and finally formed a fiber network structure via further crosslinking with solvent molecules (Fig. 1H).

Generally, an ideal biomaterial is required to be stable for storage and transportation. As show in Fig. 2A, the unchanging state proved that GAG could keep up its excellent stability for at least three months at room temperature. We also observed that GA also turned into a gel after mixing with sodium carbonate solution on the seventh day, illustrating that GA was more inclined to form a gel compared (Fig. 2B). The phenomena further illustrate the excellent stability of GAG at room temperature. More interestingly, we found that GAG showed thermal-responsiveness to the external environment, which could be due to the fact that heating decreased the hydrogelator−water interactions and hydrogelator-hydrogelator interactions (hydrogen bonding and dipole–dipole interaction), promoted the ability of water to solubilize the GAG [58]. When the heating temperature was 37 °C, the phase change would not be affected by the temperature change (Fig. S10). Subsequently, the heating temperature was gradually raised (from 25 to 70 °C). Notably, the gel phase began to change from a gel to a liquid state (Fig. 2C). As the set heating temperature became higher, the time of gel disintegration becames faster. Next, the sol−gel phase transition was further measured by the mean square displacement (MSD) curve via microrheology [59]. The temperature setting remained unchanged at 25 °C, and the GAG was heated to a transparent solution at 70 °C and
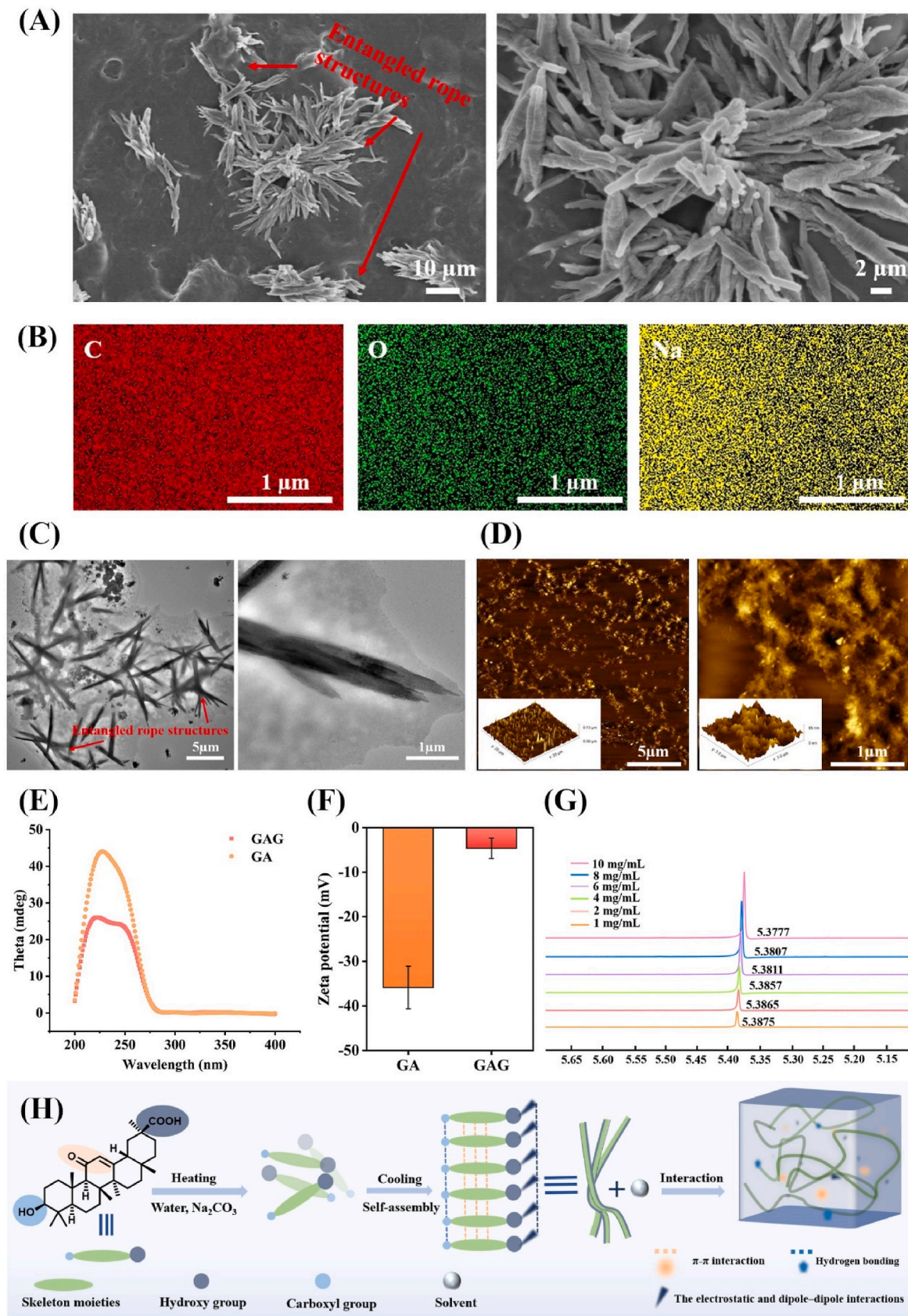
Fig. 1. The characterization and the self-assembly mechanism of the GAG. SEM images (Scale bars: 10 μm and 2 μm) (A), Corresponding elemental mapping images (Scale bars: 1 μm) (B), TEM images (Scale bars: 5 μm and 1 μm) (C), and AFM images (Scale bars: 5 μm and 1 μm) (D) of the dried GAG. E), CD spectra of free GA and GAG. F) Zeta potential of free GA and GAG. G) ^{1}H NMR spectra of various concentration of the GAG. H), Schematic diagram of the formation of the GAG.
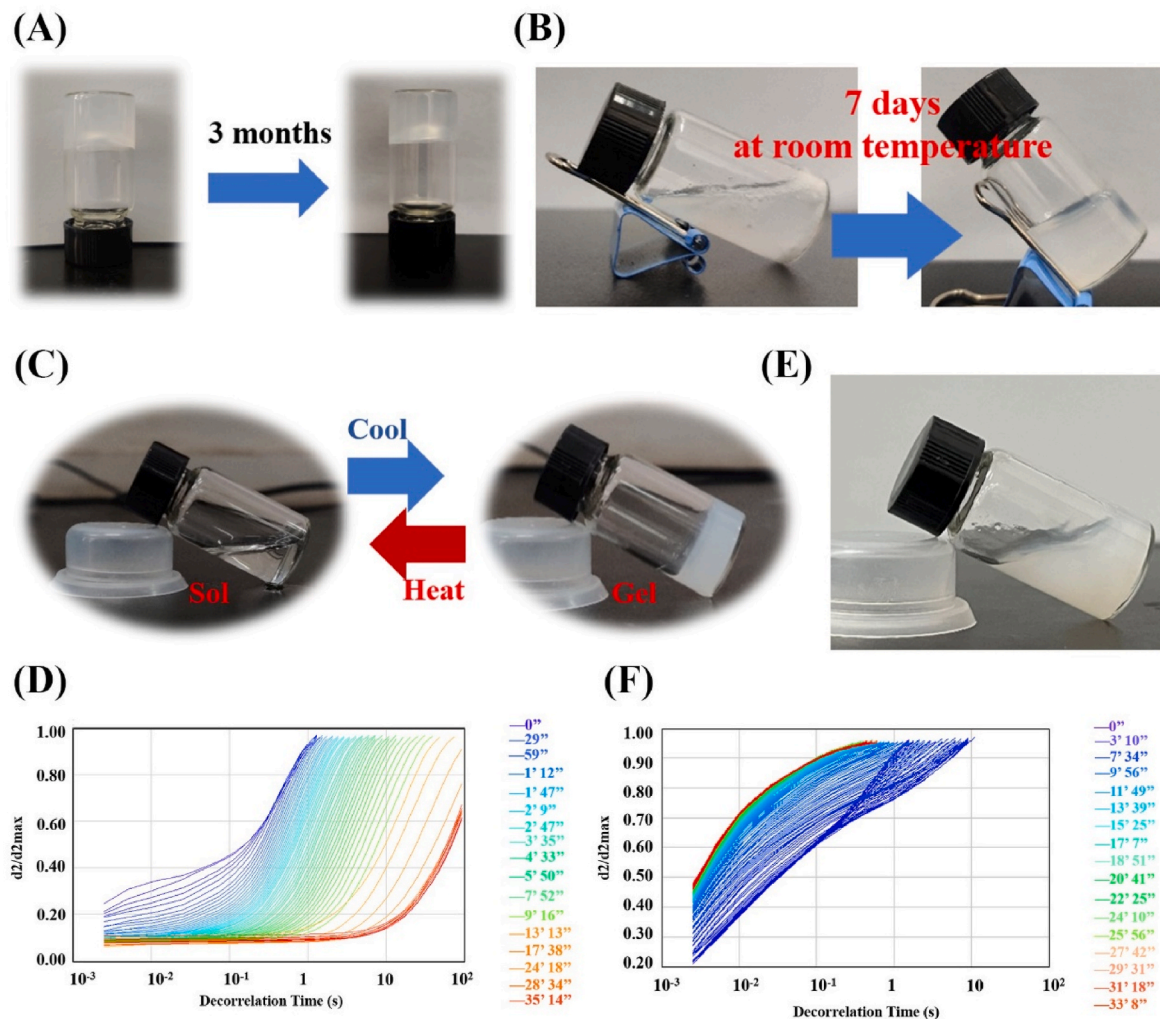
Fig. 2. The phase transition behavior of the GAG. A) Comparison of GAG before and after being placed at room temperature for 3months. B) Normal temperature mixing experiment of GAG. C) Thermo-responsiveness behavior of GAG at different temperature. D). MSD curves of GAG during the sol−gel phase transition process at 25 °C. E). Digital images of the classical test tube inversion experiment at 38 °C. F). MSD curves of GAG during the sol−gel phase transition process at 38 °C.

immediately put into the instrument to detect the phase transition process. The MSD curve moved from left to right and from top to bottom during gelation, indicating that GAG's viscoelasticity increased during the course of the process (Fig. 2D). As shown in Fig. S11, Supporting Information, the findings of the elasticity index (EI), macroscopic viscosity index (MVI), and fluidity index (FI) with respect to the test duration also indicated a considerable increase in elasticity, viscosity, and decreasing fluidity. In the meanwhile, the heated GAG solution reached the gelation threshold after just 2 min and completed the gelation process in the next 10 min before becoming stable, indicating that GAG had a good gel ability. The process of the gel collapsing was next evaluated, and the results showed that GAG's elasticity and viscosity decreased as temperature increased (Fig. S12). Continually raising the temperature eventually induced phase separation and transparent GAG solution, which produced mixed MVI and FI results at the high temperature stage. The fact that GAG existed stably at 37 °C and turned into a cloudy fluid at 40 °C drives us to explore whether there was a stable state of GAG. Since the temperature of the human body was mainly between 36.9 °C and 38.0 °C, GAG was put into the water bath at 38 °C. After heating for 10 min, the inversion tube tests showed that the GAG began to disintegrate slightly and then maintained in a semi-gel state (Fig. E). The dynamic time sweep at 38 °C demonstrated that the values of loss modulus (G′) were greater than those of storage modulus (G″), which further proved the situation described above (Fig. S13). MSD

curves of GAG at 38 °C also were essentially consistent with above results (Fig. F). All of these excellent properties could be used to create secure and effective anti-PPA therapeutics and might open up a new possibility for GAG's biomedical application and development.

3.2. Spraying properties of GAG

The administration of the spray solves the problem of non-contact drug delivery, which greatly reduces the possibility of secondary contamination during administration and also accomplishes the customization and convenience of administration [60–62]. Spray applications also offer high-throughput treatments deposition straight to the uneven surfaces of the whole target location for later sustained release [63,64]. In order to explore the spray properties of GAG, a commercially available sprayer was used in the experiment for two major goals: (1) being appropriate for future surgical operations and daily life administration; (2) dispensing in a uniform coating pattern. In further experiments, the classical test tube inversion method was proved that GAG still had the gel properties after being ejected (Fig. 3A). SEM images revealed that sprayed-GAG fibers become thinner compared to GAG (Fig. 3B). What was striking about the figures was that the pristine GAG was more inclined to aggregate into clusters, then the sprayed-GAG fibers show more dispersiveness. More evidence came from particle size analysis experiments (Fig. 3C) which also fully proved that the particle size has
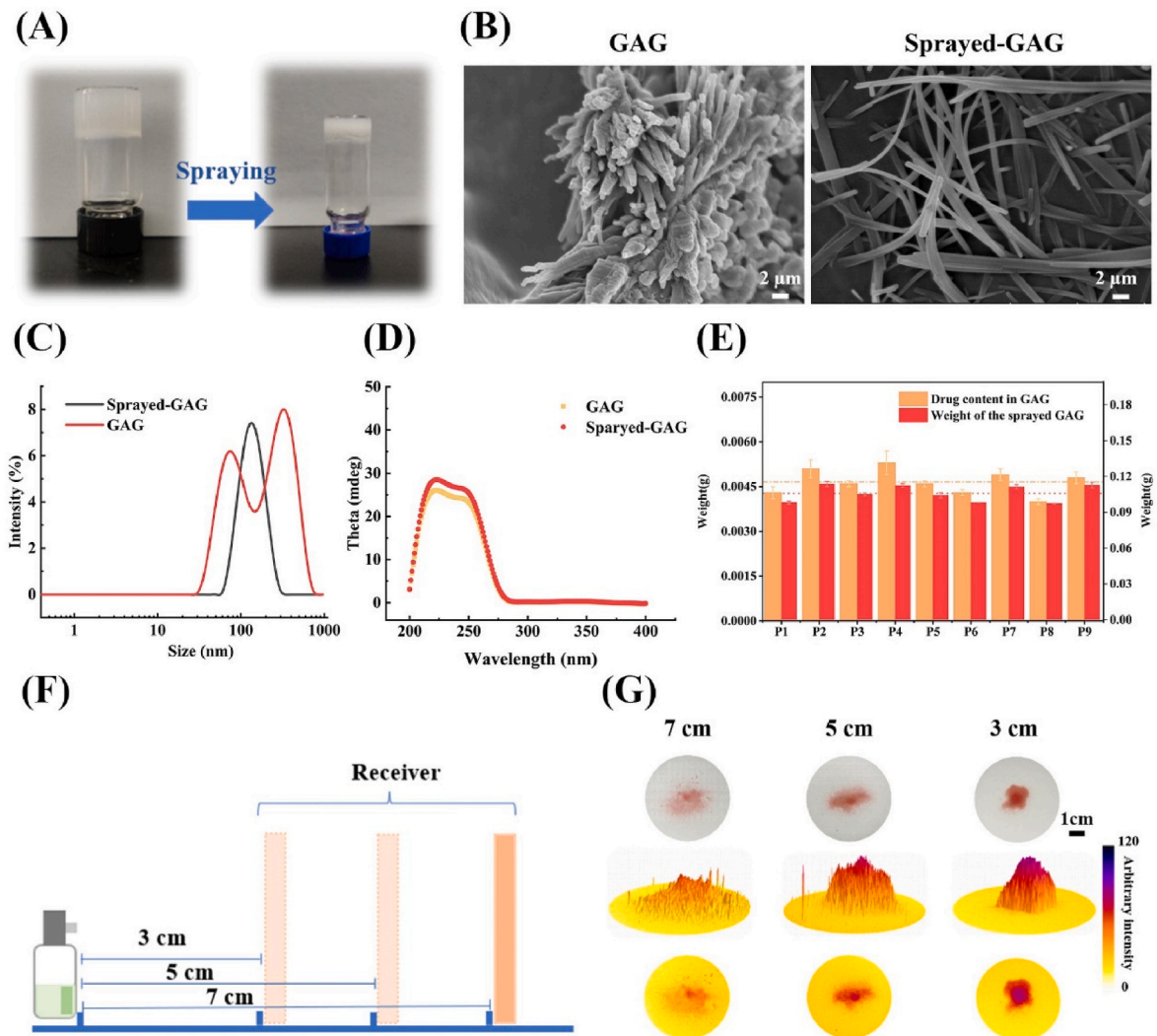
Fig. 3. General methods to examine the spray ability. A) Digital images of the classical test tube inversion experiment. B) SEM image of the GAG and the sprayed GAG, scale bar: 2 μm. C) The particle size of the GAG and the sprayed GAG. D) The CD spectra of GAG and the sprayed GAG. E) Drug content and weight of each gel ejection. (According to the order of the ejection and collection, the ejections are named P1, P2, P3, etc. The red dotted line is the average mass of GAG after ejection. The yellow dotted line is the average drug content). F) A simple device to test the uniformity of the spray gel. G) Spray-on pattern uniformity test at three different distances from the target surface, gels were dyed with 0.1 wt % allura red. (Top: Representative photographs of spray patterns taken at 7, 5, and 3 cm distances. Scale bar = 1 cm. bottom: Image-J-measured spray pattern intensity is shown in a 3D surface graphic). (For interpretation of the references to color in this figure legend, the reader is referred to the Web version of this article.)

the heterogeneity of the GAG, and sprayed - GAG had a more uniform particle size (142 nm). Nonetheless, circular dichroism results demonstrated that spraying had no effect on the molecular packing of GAG inside filaments (Fig. 3D). In FT-IR spectroscopy result and corresponding elemental mapping images (Fig. S14 and S15), there were no significant difference in the data result graph of GAG after spraying. We next aimed to further explore the influence of spraying on its rheology. The strain-dependent oscillatory shear rheology experiment (Fig. S16), the dynamic frequency sweep test (Fig. S17) and dynamic time sweep measurement (Fig. S18) indicated that spraying showed minimal impact on the rheological properties of the resulting GAG. From the above results, we believed that spraying could change the fiber homogeneity inside the gel, but do not change the way of gel accumulation, arrangement mode, the forming force and the rheological properties. In order to study the uniformity of the loading amount of each spray, we used the same sprayer for several consecutive spray experiments and collected the gel after each spray. Although each pressing strength had differences that resulted in differences in the weight of the GAG after spraying. As shown in Fig. 3E, their drug loading was roughly the same,

which further showed that we could change the amount of gel used by changing the number of sprays. To verify the homogeneous pattern formation of GAG, a simple device (Fig. 3F) was used, and the results showed that, as the distance between the sprayer and the receiving surface was getting farther and farther, the spraying area was getting larger and larger. When the distance was 3 cm, the gel was more concentrated and the color was darker due to the small spraying area. When the distance was 5 cm, the spray area was larger, the same amount of gel was distributed more widely, and the color of the distribution was lighter. As the distance increases to 7 cm, its coverage area was much larger than the former two (3 cm, 5 cm) and the color was more uniform, indicating that the thickness of the gel was more uniform (Fig. 3G). For more objective results, intensity profile of a transverse section and 3D surface plot of the spray pattern showed the intensity of spray patterns as determined by Image-J (Fig. 3G). According to this study, the distance between the sprayer and the wound during the reuse of the GAG gel could be changed to alter the size of the contact surface between the GAG gel and the wound as well as the gel's thickness. Together, these results demonstrated that the GAG may provide a general strategy to

develop a promising carrier-free drug spray in line with modern needs.

More importantly, we also assessed atomization performance of GAG after spraying with a nebulizer. As shown in Video1, Supporting Information, GAG has good atomization performance. When the concentration of GA was 28 mg/mL, the average particle size of the droplets generated by the atomization was about 4.86 μm. The atomization rate and particle size of GAG were almost unchanged as the concentration of GAG formation decreases gradually (Fig. S19). The findings of this result have a number of important implications for future lung inhalable gel.

3.3. Biocompatibility of GAG and in vitro antimicrobial activity

One important aspect influencing the use of explant biomaterials in clinics was their compatibility with blood and cells *in vivo* [65]. Compared with the previously reported sodium glycyrrhetinate [49],

the low dosage of GA and weak alkaline environment would reduce its cytotoxicity to the human body, making the topical application of GAG safer [66]. Therefore, we utilized the MTT method to evaluate the cytocompatibility of the GAG with H9c2 cells by a direct contact method. Encouragingly, MTT data showed that cell viability compared to the control group was unchanged, demonstrating the lack of cytotoxic effects (Fig. 4A). Similarly, live/dead staining analysis of cells treated in the same manner showed that after 24 h, the GAG did not make obvious toxicity to H9c2 cells (Fig. 4B). Then, a hemolysis assay with red blood cells (RBCs) was conducted to evaluate the blood compatibility. Compared with the positive control (water), the result showed that RBCs remained intact and undisrupted after incubation with GAG (Fig. 4C). Further, the hemolysis ratio calculation also showed the hemolysis ratios were less than 5%, confirming that GAG had excellent blood biocompatibility. These results supported the previous findings that GAG
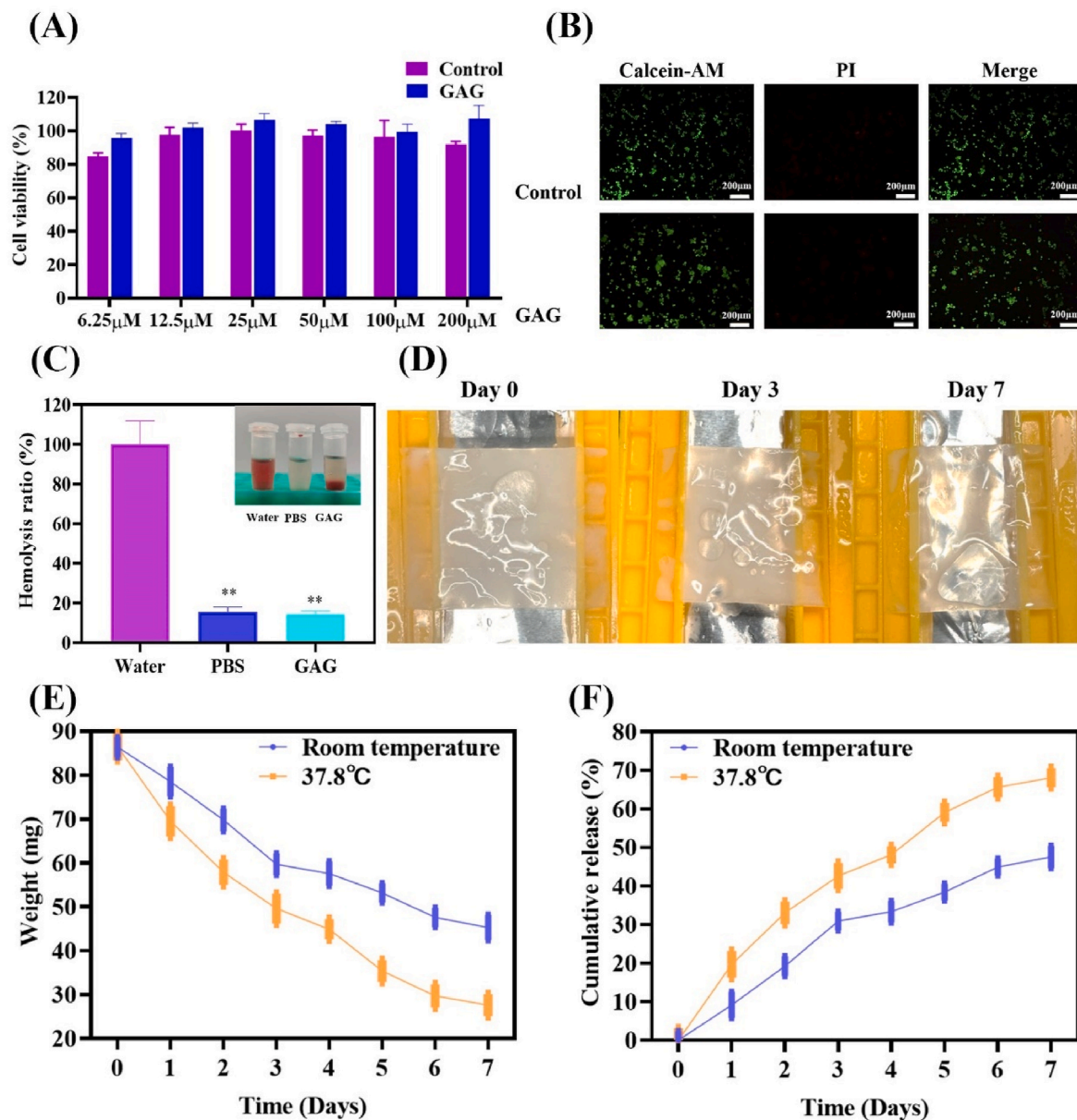

Fig. 4. GAG performed better sustainable release and lower cytotoxicity. A) MTT assay of H9c2 cells co-cultured with equal volumes of PBS and GAG. B). Live/dead staining of H9c2 cells after incubation with GAG for 24h. C) Image of the hemolytic experiment for GAG and hemolysis rate for GAG treated with RBCs for 3 h, with PBS serving as the negative control and water serving as the positive control. Photographs (D) and quantitative analysis (E) of disintegration characteristic of the GAG. F) Cumulative release profiles of the GAG. Data are presented as the mean ± SEM (n = 3). *represents P < 0.05, **represents P < 0.01 *** represents P < 0.001 show the significant differences.

showed low cytotoxicity and strong hemocompatibility with mammalian cells.

In order to reduce the negative effects brought by the foreign body response and the degradation byproducts, the biodegradation duration of barrier material has become a crucial consideration for anti-PPA treatments [67,68]. As we all know, the barrier material needs to remain in the wound for the crucial phase of adhesion formation (3–5 days after operation) [69]. Based on the thermal sensitivity of GAG described above, we speculated that this response performance could help it disintegration in the body within 3–5 days, so as to better exert its treatment effect. In order to test this hypothesis, the *in vitro* disintegration behavior of the hydrogel was studied further. Fig. S20 indicated that PBS would not affect the stability of GAG. Because the human abdominal cavity temperature is approximately 37.8 °C, two groups GAG (1 mL)
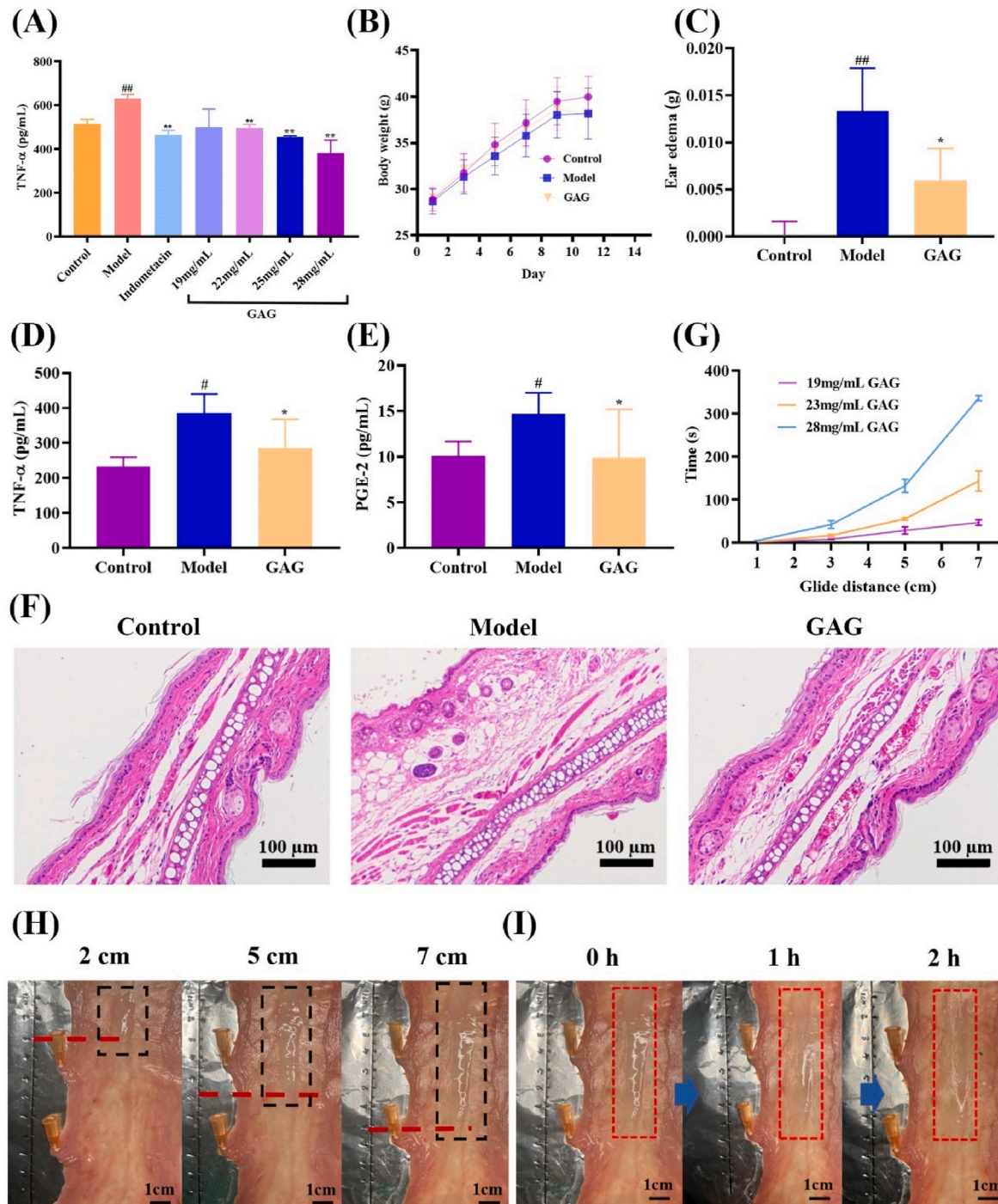

Fig. 5. A) Effect of GAG on contents of TNF-α in LPS-induced RAW 264.7 cells. B) The average weight of mice in various groups. C) Effect of GAG on xylene-induced ear edema test. TNF-α (D) and PGE-2 (E) in the mouse ear tissue. F) Xylene-induced mouse ear tissue histopathological analysis. Scale bar:100 μm. G) The time required for different concentrations (19 mg/mL, 23 mg/mL, 28 mg/mL) of GAG to slide the same distance. H) Digital photos of the sliding process (2 cm, 5 cm, 7 cm respectively) of GAG on the inclined intestine surface. Scale bar:1 cm. I) 1 h and 2 h later, digital photos of GAG (GA:28 mg, Na$_2$CO$_3$: 0.075 mol/L, 1 mL) after gliding on the intestine surface. Scale bar:1 cm. All of data above are presented as mean ± SD (n = 7). $^{\#\#}$p < 0.01 compared to the model group with the control group. *represents P < 0.05, **represents P < 0.01 of GAG group VS model group, respectively.

were sprayed in dialysis bags and put into PBS solution at 37.8 °C and room temperature, respectively, and photographs were taken to document the existence state. At certain intervals, we took out the dialysis bags, took pictures, recorded, and observed the remaining amounts of gels. Not unexpectedly, as shown in Fig. 4D, the contents of the dialysis bags decreased over time, whether at room temperature or 37.8 °C. Compared with day 0, the gel weight in the dialysis bags was significantly less on days 7 and 3, and the trend was gradually decreasing (Fig. 4E). In addition, we further conducted an experiment to examine that increasing temperature would encourage the breakdown of GAG and the release of GA (Fig. 4F). These results demonstrated that the GAG could exist throughout the process of intestinal adhesion formation, insulate the injured tissue, and then slowly release GA to play an anti-inflammatory effect.

Bacterial infection could result in life-threatening consequences that induce the multiple organ failure and death. The sprayed and contactless administration could reduce local contamination but could not completely avoid abdominal infection. Therefore, considering the inherent antibacterial activity of GA, it might be significative for GAG to play an auxiliary antibacterial role. Generally, Gram-positive *S. aureus* and Gram-negative *E. coli* are two major causes of hospitalization-related infections. Considering the inherent antibacterial ability [57], antibacterial activity of the prepared GAG was tested on *S. aureus* and *E. coli* by colony-forming unit (CFU) methods [51]. Encouragingly, GAG inhibited *S. aureus* proliferation in a dose-dependent manner and could inhibit the reproduction of *S. aureus.* at 200μg/mL^{-1} (Fig. S21 and Fig. S22), which might be due to the GA moiety of GAG could inhibit the uptake of nutrients via causing alterations in the expression of genes related to nutrient metabolism and modulate virulence via controlling the expression of several virulence factor [70,71]. At the *E. coli* group, a sizable proportion of colony-forming units (CFU) of still-viable bacteria were still visible in the GAG group (Fig. S21). The result of this research above could be supported by the previous experiment result that GA was not inhibitory against *E. coli* [72]. Considering all of the data, the results demonstrate that GAG exhibited great selective efficiency against Gram-positive *S. aureus.* Exposure of tissues to airborne and instrumental microorganisms is inevitable during gastrointestinal surgery. The selective antimicrobial activity of the GAG might be a beneficial quality for preventing infection after severe abdominal injuries.

3.4. In vitro anti-inflammatory and the ear edema test

Lipopolysaccharide (LPS)-induced RAW 264.7 cells were used as an *in vitro* inflammatory model to evaluate the anti-inflammatory effects of GAG. After LPS stimulation, the supernatant of the model group contained significantly more tumor necrosis factor-α (TNF-α) than that of control group, showing that the amount of TNF-α released by macrophages was significantly increased (Fig. 5A). In addition, the findings confirmed the pattern that had been seen up to that point, showing that as GAG concentration rose, TNF-α concentration fell. The difference was considerable, especially between the model group, the positive group and the GAG group, showing that the 28 mg/mL GAG was more effective than the positive group and could further prevent inflammatory cells from releasing TNF-α. To further examine the anti-inflammatory ability, xylene-induced ear edema test for assessing the anti-inflammatory activities of drugs, was carried out [73]. It has always been thought that a change in body weight during treatment indicates *in vivo* toxicity. No appreciable weight loss was observed, demonstrating that the locally administered GAG had no adverse effects (Fig. 5B). In addition, compared to the control group (Fig. 5C), GAG had a significant (P < 0.05) inhibitory effect on the auricle swelling of mice induced by xylene indicating that GAG remarkably suppressed acute inflammation *in vivo*. TNF-α and other proinflammatory cytokines, to our understanding, play important roles in the inflammatory process. Prostaglandin E2 (PEG-2) is typically a crucial pro-inflammatory mediator involved in all major signs of inflammation: edema, redness, swelling and pain. We found that

TNF-α (Fig. 5D) and PEG-2 (Fig. 5E) levels were reduced by GAG in rat models of inflammation brought on by xylene. Additional histopathological examination of ear tissue sections revealed that xylene-induced edema and inflammatory cell infiltration in the ear tissue were significantly reduced (Fig. 5F). In the blank group, the ear tissue of mice was complete in morphology and structure, with a thin layer of stratum corneum on the surface, clear epidermal structure, little difference in thickness, less thin subcutaneous connective tissue, and distribution of capillaries and nerves. The auricle cartilage was parallel to the skin. No other obvious pathological changes were found; the model group mice's ears were noticeably thicker, and there was edema in the auricular subcutaneous tissue; the connective tissue was sparsely arranged, the transmittance was enhanced, and there were more inflammatory cells infiltrated in the subcutaneous tissue, mainly lymphocytes and neutrophils. The edema of the subcutaneous tissue of the auricle of the mice in the administration group and the number of infiltrated inflammatory cells were significantly relieved and decreased compared to the model group. In addition, we also tested the anti-inflammatory activity of low concentrations of GAG (GA:19 mg, Na$_2$CO$_3$: 0.075 mol/L, 1 mL) (Fig. S23), showing that low concentrations of GAGs are less effective than high concentrations (GA:28 mg, Na$_2$CO$_3$: 0.075 mol/L, 1 mL). This was exactly in line with our previous speculation that the GAG (GA:28 mg, Na$_2$CO$_3$: 0.075 mol/L) had a better therapeutic effect to treat inflammation.

3.5. In vivo anti-adhesion test

Pharmaceutical studies have been proved that anti-inflammatory drugs have been adopted clinically using to prevent postoperative adhesion. The *in vitro* studies above-mentioned, including, stability study, disintegration experiment and spray characteristics test, demonstrated that the GAG was a promising candidate as barrier material. Herein, the GAG was further investigated in relation to the treatment effect of PPA. Because effective retention on target tissues in body fluids and better regulated degradation profiles depend on organ-adhesive performance. We firstly assessed the ability of the GAG bind to the surface of intestine surface obtained from a pig. Taking into account the gaps between adjacent intestines and the curvature of the intestines themselves, the different concentration of GAG droplet (0.2 mL) was placed on the inclined intestine surface (30°) and their sliding time and distance relationship was recorded (Fig. S24). the GAG could slide on the surface of the intestine and has a certain amount of retention in the initial position, evidencing the ability of GAG to adhere the surface of intestine surface (Fig. 5G and H). It was probably because the GAG was negatively charged and was rich in oxygen-containing groups (carboxyl group, carboxy and hydroxyl groups), which were conducive for the GAG to attach the proteins with a positive charge by hydrogen bonds and electrostatic interaction [74–76]. Compared with low concentration (GA:19 mg/mL, Na$_2$CO$_3$: 0.075 mol/L) and medium concentration (GA:23 mg/mL, Na$_2$CO$_3$:0.075 mol/L) of GAG, GAG (GA:28 mg/mL, Na$_2$CO$_3$:0.075 mol/L) took longer to slide the same distance, further indicating that 28 mg/mL GAG possessed greater viscosity and was more suitable to be used as ideal material (Fig. 5G). We then sought to assess the effects of spraying on GAG's capacity for adhesion (Fig. 5H and I). As we expected, the sprayed GAG was evenly distributed on the surface of the intestine at first, and after 2 h, the area of GAG became larger and formed a gel film on the surface of the intestine. These obtained results provided a foundation for the new treatment strategy of intestinal adhesions. To control the inflammatory reactions and further relieve the development of PPA, GAG was used in an *in vitro* adhesion formation model. As shown in Fig. 6A, layer by layer, the abdominal cavity was dissected to expose the natural abdominal wall and cecum. The cecum was scraped until macular hemorrhage formed after the abdominal wall was made defective. The GAG (1 mL) spray was then evenly applied to each defect location to isolate the defective cecum and abdominal wall of each rat (Video 2, Supporting Information). Control was sterile
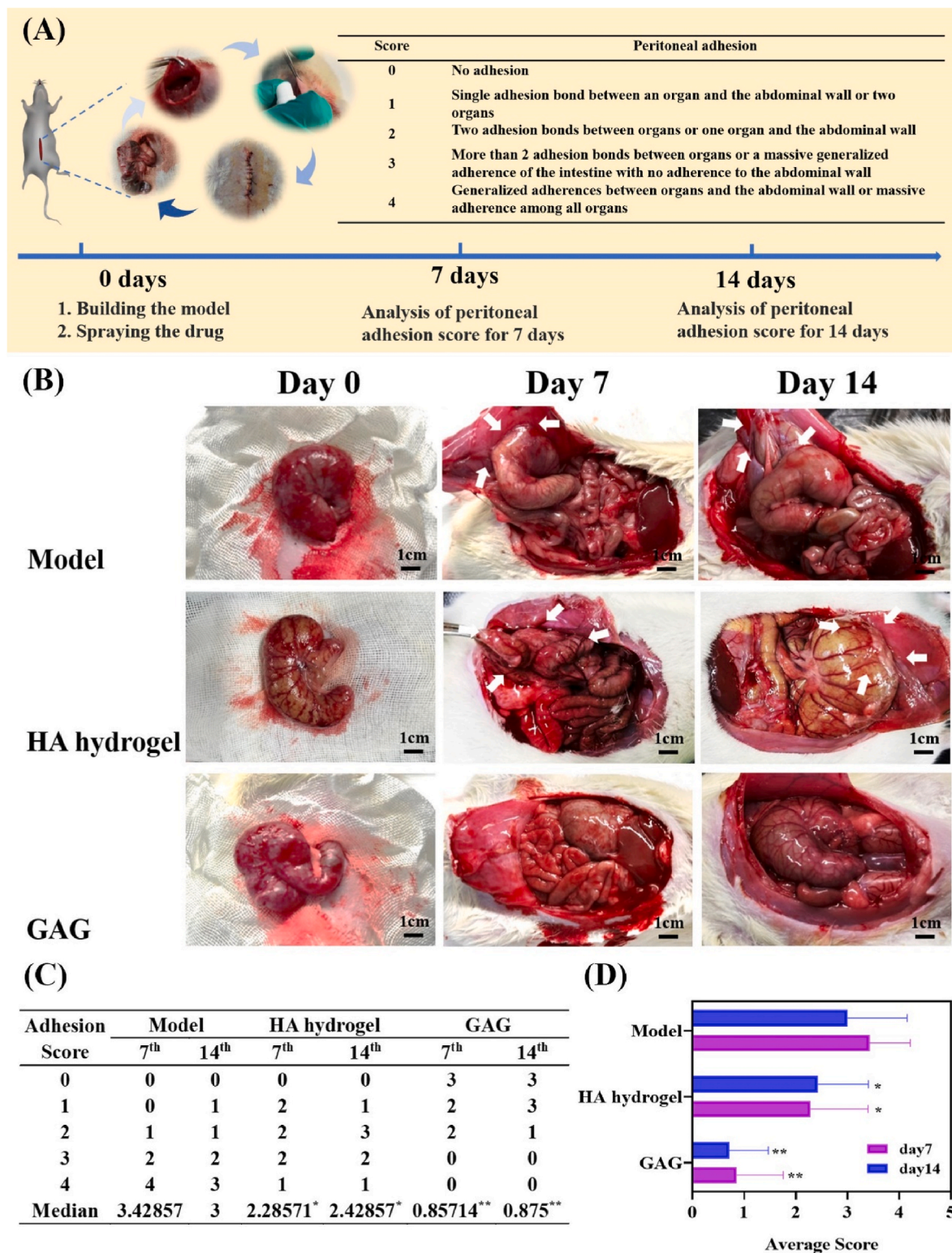
Fig. 6. Post-surgery antiadhesion efficacy of GAG in a model with rat side wall defect and cecum abrasion. A) A schematic showing the treatment for the sidewall defect-cecum abrasion and peritoneal adhesion score. B) Digital photos of the cecum and abdominal side wall 0, 7, and 14 days aftertreatment (white arrows indicated adhesion sites between the abdominal wall and cecum). Adhesion scores of different groups after treatment on day 7 (C) and day 14 (D) postoperation. All of data above are presented as mean ± SD (n = 7). *represents P < 0.05, **represents P < 0.01.

normal saline. Simultaneously, as a positive control group, 1 mL commercial hyaluronic acid (HA) hydrogel was injected onto the injured abdominal wall and damaged cecum. The abdominal cavity was then stitched layer by layer.

The adhesion between the abdominal wall and the cecum of rats was examined on 7 days following surgery. In the GAG group, the absence of any GAG remnants in the abdominal cavity proved that the substance had totally broken down, illustrating that it fulfilled its function as an effective adhesive-prevention barrier and has good degradability in the animal body. Fig. 6B, C, and D showed examples of gross observation

images of adhesion formation and adhesion scores. Strong adhesion between the peritoneum and cecum was present in all of the rats in the control group, where the proximal omentum, adjacent mesentery, and adipose tissues, as well as a significant portion of the peritoneal epidermis, were all tightly adhered. Moreover, all of the rats (n = 7) had adhesion scores more than or equal to 3. For the group treated with HA hydrogel, rats still suffered from peritoneal adhesions scored at 2.28571, showing the clinical used HA hydrogel could only reduce the postoperative adhesions to some extent. Conversely, as a result of the GAG's barrier effect, the GAG group exhibited moderate adhesion with minimal bridging around the peritoneum and cecum. The adhesion score of the rats was equal to 0.857, which was much lower than that of HA hydrogel and model groups, indicating a perfect prevention rate with no

adhesion (P < 0.05, Fig. 6C). After treatment for 2 weeks (Fig. 6B, C, D), the adhesions between the abdominal wall and injured cecum were also plainly visible in the control group. The sticky sites could not be separated by minor straining unless using sharp instruments to peel off the adhesive area. Compared to the control group on 7days, the extent of the adhesions expanded to some extent over time. In the commercial HA hydrogel group, the result could be clearly observed that the HA hydrogel could only partially alleviate the adhesion with a score of 2.42857, indicating the unsatisfactory anti-adhesion efficiency of commercial HA hydrogel. By contrast, for the GAG group, most rats (n = 3) showed no tissue adhesion. Importantly, the bleeding points and defects resulting from model establishment completely disappeared and had almost recovered. Both the damaged cecum and the abdominal wall
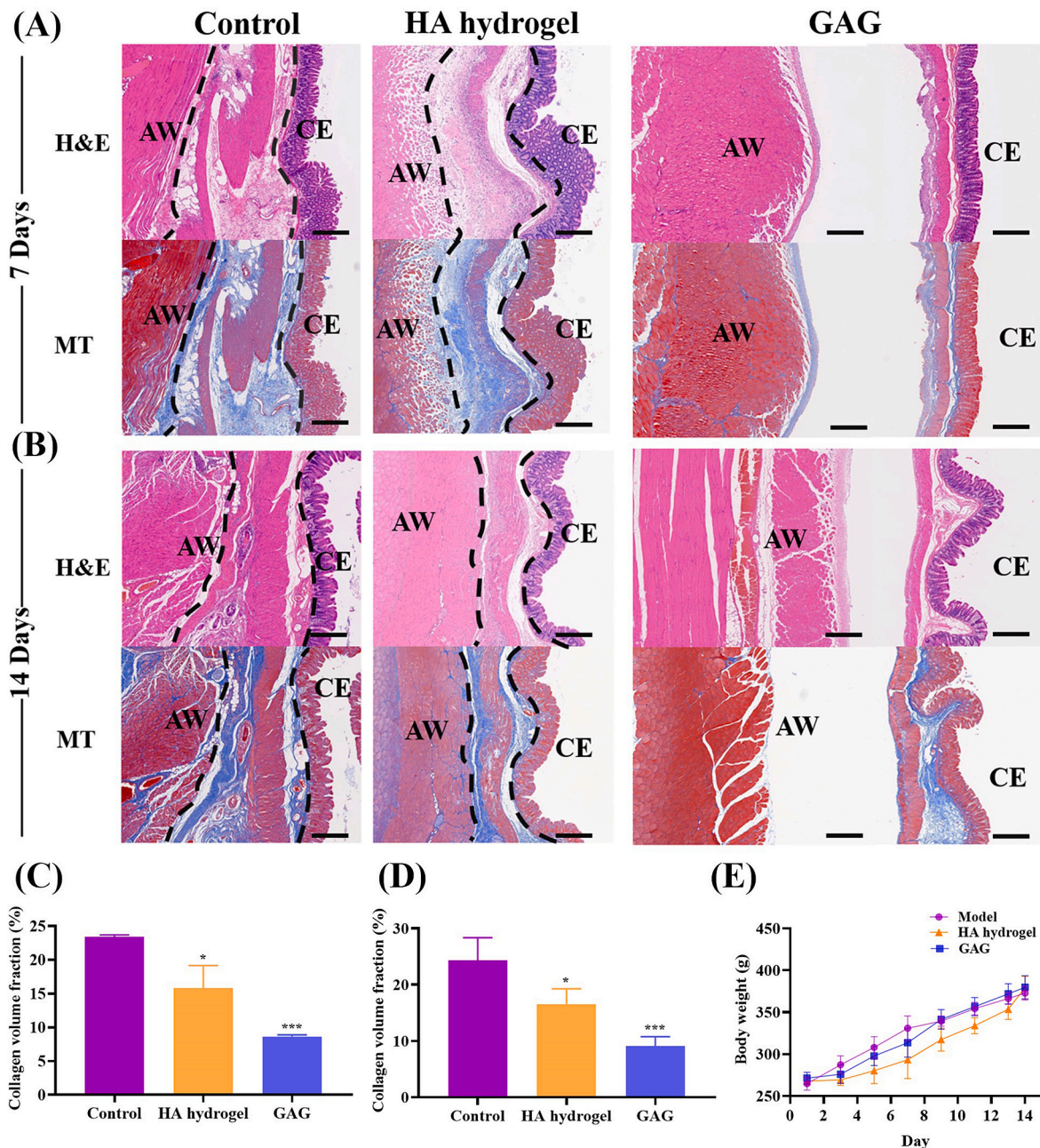

Fig. 7. H&E staining and MT staining were used to analyze the histopathology of samples from the control, HA hydrogel and GAG-treated groups on days 7 (A) and 14 (B) following surgery. AW: the surface of the abdominal wall. CE: surface of the cecum. The adhesion area in the control group was represented by red dotted lines. Scale bars: 400 μm. Statistical analysis of collagen deposition on days 7 (C) and 14 (D). E) The weight of mice in different groups. The bar graphs represent mean +SD (n = 3), *represents P < 0.05, **represents P < 0.01. *** represents P < 0.001 show the significant differences. (For interpretation of the references to color in this figure legend, the reader is referred to the Web version of this article.)

were fully repaired. The adhesion score of the GAG group (0.875) was lower than the other adhesion scores of two groups (3 and 2.42857, respectively), supporting the anti-adhesion efficacy of the GAG.

The mucosa, submucous membrane, and muscle layer are the primary locations of the early inflammatory response of abdominal adhesions. As seen by H&E staining, inflammatory cells were recruited in the three groups (Fig. 7A and B). For the control group, the injured cecum's smooth muscles and the harmed abdominal wall were united on day 7. Additionally, there were many inflammatory cells, such as neutrophils, macrophages, and lymphocytes. The commercial HA hydrogel can only decrease inflammation to a limited level in the HA hydrogel group. In comparison to the control group, the inflammatory and congestive responses were significantly reduced after GAG therapy. These findings demonstrated that the product GA produced by GAG disintegration might reduce inflammation in the cecum and damaged abdominal wall. One of the key elements in the development of fibrous adhesion was the deposition of collagen. Masson trichrome (MT) staining, which showed the deposition of collagen (stained blue in the adhesion region), revealed strong attachment of the abdominal wall and cecum mucosa in the control group (Fig. 7A, B, C). Furthermore, a mild fibroproliferative response, connective tissue fibrosis, collagen deposition, and collagen volume fraction in the adhesion sites suggested that the commercial HA hydrogel simply exerted a limited therapeutic effect on postoperative adhesions. As opposed to the control group and HA hydrogel group, the injured abdominal wall and cecum in GAG group were evaluated independently owing to the poor adhesion. The injured areas showed signs of fibroblasts and collagen fibers, and the defected abdominal wall was repaired with new peritoneal mesothelium. In addition, the GAG-treated the injured abdominal wall and cecum showed a lower collagen volume fraction ((Fig. 7C). In the control group, H&E staining (Fig. 7A, B, D) after 14 days revealed that the injured cecal muscular layer and the muscles of the abdominal wall were fused by connective tissue with a significant amount of inflammatory cells, indicating that inflammation and the formation of adhesions were closely related processes. There was still noticeable dense collagen deposition between the harmed cecum and the harmed abdominal wall in the control group. For the HA hydrogel group, H&E staining and MT staining indicated that the degree of adhesion was alleviated to some extent, indicating its poor prevention effect on the recurrent adhesions. The GAG group, however, showed pathological evidence of weak adhesion and a lesser collagen volume fraction (Fig. 7D). And the epithelial structures of the abdominal wall and the cecum were completely reconstructed. These results provided additional evidence that the GAG could successfully and consistently avoid the abdominal cecum adhesion. An ideal anti-adhesion material would not only operate as a barrier with a proper therapeutic effect but it would also not be poisonous to the organ toxicity. On day 7 and day 14 postoperation, as shown in Fig. 7E, the increase in body weight among the rats in each group suggested that GAG had no unfavorable consequences on the health. Compared with the normal tissue, in the GAG group, there was no significant change in histology between day 7 and day 14 after treatment (Fig. S25). The deposition of collagen also was similar to normal tissue, further demonstrating that the GAG was biocompatible and did not show any negative effects for local tissue. On the basis of the above results, the GAG was a potential material for the prevention of intraperitoneal adhesion.

The primary contributors to peritoneal adhesion during surgery were the unavoidable peritoneal damage, inflammatory response, and the risk of infection. Furthermore, the entire process of adhesion creation involves the inflammatory reaction. To stop the development of fibrin and the migration of inflammatory cells from other wound sites, a viable alternative barrier material with excellent biodegradability also should be placed over irregular wound sites. On the basis of the above results, the aforementioned factors must be taken into account when preventing postoperative peritoneal adhesion. Fortunately, the GAG was basically in line with the points mentioned above and the following explanations might be used to explain this phenomenon: (1) Owing to good spraying

characteristic, the GAG could avoid wound foreign body contaminants pollution carried by instruments during drug delivery. The inborn antibacterial activity might be a beneficial assistant for help kill intraperitoneal microbial infected during surgery. (2) After sprayed, the GAG could rapidly form a thin hydrogel film in tissue surface and completely cover the peritoneum injury surface, physically isolating the injury sites from neighboring tissues. At the same time, it could exist throughout the process of intestinal adhesion formation (3–5 days after operation) to reduce contact between injured tissues. The stable GAG could further form a drug depot in the lesion tissue and be completely disintegrated to slowly self-releases GA within seven days. (3) Its good biocompatibility could ensure the GAG without causing a secondary inflammatory reaction. Furthermore, on account of anti-inflammatory effects of natural GA, GAG also could the inflammatory response on the damaged surface including inflammatory cells infiltration. All of which might have critical roles in preventing adhesion and subsequent adhesion following adhesiolysis. Together, these findings illustrated that the GAG had the capacity to manage and deter postoperative adhesions between biological interfaces.

4. Conclusion

In summary, this study aimed to achieve a biosafe, biodegradable, low toxic but highly effective and therapeutically accessible transformed material to prevent the development of peritoneal adhesion following surgery. In this strategy, the GAG was easily developed by combining glycyrrhetinic acid and sodium carbonate solution and exhibited promising self-healing, anti-inflammatory activity, biodegradability. The results of the biocompatibility and antibacterial tests also demonstrated that this easy-assembled GAG had outstanding antibacterial activities against *S. aureus* with no cytotoxicity. In particular, the spray ability of GAG realized the convenience of drug delivery and the dose could be customized according to the patient's own conditions. Moreover, a model for sidewall defects and cecum abrasion was developed. It was discovered that the GAG may serve as a physical barrier material as well as an additional therapeutic medication, significantly reducing the formation of postoperative peritoneal adhesions by reducing inflammatory reactions and collagen fiber deposition. The current research would therefore be an effective method of preventing peritoneal adhesions and has promising clinical applications for this goal.

Credit author statement

Linjun Zou: Writing-Original draft preparation, Conceptualization, Methodology; Yong Hou: Investigation, Writing-review & editing; Jiawen Zhang: Software, Supervision; Meiying Chen: Data curation, Validation; Peiying Wu: Validation, Formal analysis; Changcun Feng: Visualization, Software; Qinglong Li: Methodology, Data curation; Xudong Xu: Investigation, Resources; Zhaocui Sun: Methodology, Investigation; Guoxu Ma: Resources, Project administration.

Declaration of competing interest

The authors declare that they have no known competing financial interests or personal relationships that could have appeared to influence the work reported in this paper.

Data availability

The data that has been used is confidential.

Acknowledgements

Appendix A. Supplementary data

Supplementary data related to this article can be found at https://doi.org/10.1016/j.mtbio.2023.100755.

References

[1] Q. Guo, H. Sun, X. Wu, Z. Yan, C. Tang, Z. Qin, M. Yao, P. Che, F. Yao, J. Li, In situ clickable purely zwitterionic hydrogel for peritoneal adhesion prevention, Chem. Mater. 32 (15) (2020) 6347–6357.

[2] J. Gao, J. Wen, D. Hu, K. Liu, Y. Zhang, X. Zhao, K. Wang, Bottlebrush inspired injectable hydrogel for rapid prevention of postoperative and recurrent adhesion, Bioact. Mater. 16 (2022) 27–46.

[3] L.M. Stapleton, H.J. Lucian, A.K. Grosskopf, A.A.A. Smith, K.P. Totherow, Y. J. Woo, E.A. Appel, Dynamic hydrogels for prevention of post-operative peritoneal adhesions, Adv. Therapeut. 4 (3) (2021).

[4] S. Soltany, Postoperative peritoneal adhesion: an update on physiopathology and novel traditional herbal and modern medical therapeutics, N. Schmied. Arch. Pharmacol. 394 (2) (2020) 317–336.

[5] J. Zindel, J. Mittner, J. Bayer, S.L. April-Monn, A. Kohler, Y. Nusse, M. Dosch, I. Buchi, D. Sanchez-Taltavull, H. Dawson, M. Gomez de Aguero, K. Asahina, P. Kubes, A.J. Macpherson, D. Stroka, D. Candinas, Intraperitoneal microbial contamination drives post-surgical peritoneal adhesions by mesothelial EGFR-signaling, Nat. Commun. 12 (1) (2021) 7316.

[6] B. Schnuriger, G. Barmparas, B.C. Branco, T. Lustenberger, K. Inaba, D. Demetriades, Prevention of postoperative peritoneal adhesions: a review of the literature, Am. J. Surg. 201 (1) (2011) 111–121.

[7] C.C. Fang, T.H. Chou, J.W. Huang, C.C. Lee, S.C. Chen, The small molecule inhibitor QLT-0267 decreases the production of fibrin-induced inflammatory cytokines and prevents post-surgical peritoneal adhesions, Sci. Rep. 8 (1) (2018) 9481.

[8] K. Ota, K. Sato, J. Ogasawara, T. Takahashi, H. Mizunuma, M. Tanaka, Safe and easy technique for the laparoscopic application of Seprafilm(R) in gynecologic surgery, Asian J. Endosc. Surg. 12 (2) (2019) 242–245.

[9] X. Song, Z. Zhang, Z. Shen, J. Zheng, X. Liu, Y. Ni, J. Quan, X. Li, G. Hu, Y. Zhang, Facile preparation of drug-releasing supramolecular hydrogel for preventing postoperative peritoneal adhesion, ACS Appl. Mater. Interfac. 13 (48) (2021) 56881–56891.

[10] J. Zhou, H. Zhang, M.S. Fareed, Y. He, Y. Lu, C. Yang, Z. Wang, J. Su, P. Wang, W. Yan, K. Wang, An injectable peptide hydrogel constructed of natural antimicrobial peptide J-1 and ADP shows anti-infection, hemostasis, and antiadhesion efficacy, ACS Nano 16 (5) (2022) 7636–7650.

[11] Z. Li, L. Liu, Y. Chen, Dual dynamically crosslinked thermosensitive hydrogel with self-fixing as a postoperative anti-adhesion barrier, Acta Biomater. 110 (2020) 119–128.

[12] J. Tang, Z. Xiang, M.T. Bernards, S. Chen, Peritoneal adhesions: occurrence, prevention and experimental models, Acta Biomater. 116 (2020) 84–104.

[13] R.M. Leclercq, K.W. Van Barneveld, M.H. Schreinemacher, R. Assies, M. Twellaar, N.D. Bouvy, J.W. Muris, Postoperative abdominal adhesions and bowel obstruction. A survey among Dutch general practitioners, Eur. J. Gen. Pract. 21 (3) (2015) 176–182.

[14] V.B. Rahimi, R. Shirazinia, N. Fereydouni, P. Zamani, S. Darroudi, A.H. Sahebkar, V.R. Askari, Comparison of honey and dextrose solution on post-operative peritoneal adhesion in rat model, Biomed. Pharmacother. 92 (2017) 849–855.

[15] Q. Hu, X. Xia, X. Kang, P. Song, Z. Liu, M. Wang, W. Guan, S. Liu, A review of physiological and cellular mechanisms underlying fibrotic postoperative adhesion, Int. J. Biol. Sci. 17 (1) (2021) 298–306.

[16] W.M. van Grevenstein, L.J. Hofland, M.E. van Rossen, P.M. van Koetsveld, J. Jeekel, C.H. van Eijck, Inflammatory cytokines stimulate the adhesion of colon carcinoma cells to mesothelial monolayers, Dig. Dis. Sci. 52 (10) (2007) 2775–2783.

[17] Y.C. Cheong, G. Premkumar, M. Metwally, J.L. Peacock, T.C. Li, To close or not to close? A systematic review and a meta-analysis of peritoneal non-closure and adhesion formation after caesarean section, Eur. J. Obstet. Gynecol. Reprod. Biol. 147 (1) (2009) 3–8.

[18] M. Ghadiri, V. Baradaran Rahimi, E. Moradi, M. Hasanpour, C.C.T. Clark, M. Iranshahi, H. Rakhshandeh, V.R. Askari, Standardised pomegranate peel extract lavage prevents postoperative peritoneal adhesion by regulating TGF-β and VEGF levels, Inflammopharmacology 29 (3) (2021) 855–868.

[19] S. Chiorescu, O.A. Andercou, N.O. Grad, I.A. Mironiuc, Intraperitoneal administration of rosuvastatin prevents postoperative peritoneal adhesions by decreasing the release of tumor necrosis factor, Clujul Med. 91 (1) (2018) 79–84.

[20] P. Rahmanian-Devin, H. Rakhshandeh, V. Baradaran Rahimi, Z. Sanei-Far, M. Hasanpour, A. Memarzia, M. Iranshahi, V.R. Askari, X. Cui, Intraperitoneal lavage with crocus sativus prevents postoperative-induced peritoneal adhesion in a rat model: evidence from animal and cellular studies, Oxid. Med. Cell. Longev. 2021 (2021) 1–22.

[21] D. Babadi, S. Rabbani, S. Akhlaghi, A. Haeri, Curcumin polymeric membranes for postoperative peritoneal adhesion: comparison of nanofiber vs. film and phospholipid-enriched vs. non-enriched formulations, Int. J. Pharm. 614 (2022).

[22] C. Brochhausen, V.H. Schmitt, A. Mamilos, C. Schmitt, C.N.E. Planck, T.K. Rajab, H. Hierlemann, C.J. Kirkpatrick, Expression of CD68 positive macrophages in the use of different barrier materials to prevent peritoneal adhesions—an animal study, J. Mater. Sci. Mater. Med. 28 (1) (2016).

[23] F. Cheng, F. Wu, H. Li, T. Yan, X. Wei, G. Wu, J. He, Y. Huang, Biodegradable N, O-carboxymethyl chitosan/oxidized regenerated cellulose composite gauze as a barrier for preventing postoperative adhesion, Carbohydr. Polym. 207 (2019) 180–190.

[24] S.M. Mayes, J. Davis, J. Scott, V. Aguilar, S.A. Zawko, S. Swinnea, D.L. Peterson, J. G. Hardy, C.E. Schmidt, Polysaccharide-based films for the prevention of unwanted postoperative adhesions at biological interfaces, Acta Biomater. 106 (2020) 92–101.

[25] J. Zheng, R. Fan, H. Wu, H. Yao, Y. Yan, J. Liu, L. Ran, Z. Sun, L. Yi, L. Dang, P. Gan, P. Zheng, T. Yang, Y. Zhang, T. Tang, Y. Wang, Directed self-assembly of herbal small molecules into sustained release hydrogels for treating neural inflammation, Nat. Commun. 10 (1) (2019) 1604.

[26] H. Li, X. Wei, X. Yi, S. Tang, J. He, Y. Huang, F. Cheng, Antibacterial, hemostasis, adhesive, self-healing polysaccharides-based composite hydrogel wound dressing for the prevention and treatment of postoperative adhesion, Mater. Sci. Eng. C. Mater. Biol. Appl. 123 (2021) 111978.

[27] J. Yu, K. Wang, C. Fan, X. Zhao, J. Gao, W. Jing, X. Zhang, J. Li, Y. Li, J. Yang, W. Liu, An ultrasoft self-fused supramolecular polymer hydrogel for completely preventing postoperative tissue adhesion, Adv. Mater. 33 (16) (2021).

[28] G.U. Ruiz-Esparza, X. Wang, X. Zhang, S. Jimenez-Vazquez, L. Diaz-Gomez, A. M. Lavoie, S. Afewerki, A.A. Fuentes-Baldemar, R. Parra-Saldivar, N. Jiang, N. Annabi, B. Saleh, A.K. Yetisen, A. Sheikhi, T.H. Jozefiak, S.R. Shin, N. Dong, A. Khademhosseini, Nanoengineered shear-thinning hydrogel barrier for preventing postoperative abdominal adhesions, Nano-Micro Lett. 13 (1) (2021) 212.

[29] G. Wei, Z. Wang, R. Liu, C. Zhou, E. Li, T. Shen, X. Wang, Y. Wu, X. Li, A combination of hybrid polydopamine-human keratinocyte growth factor nanoparticles and sodium hyaluronate for the efficient prevention of postoperative abdominal adhesion formation, Acta Biomater. 138 (2022) 155–167.

[30] H. Zeng, X. Liu, Z. Zhang, X. Song, J. Quan, J. Zheng, Z. Shen, Y. Ni, C. Liu, Y. Zhang, G. Hu, Self-healing, injectable hydrogel based on dual dynamic covalent cross-linking against postoperative abdominal cavity adhesion, Acta Biomater. 151 (2022) 210–222.

[31] Y. Hou, L. Zou, Q. Li, M. Chen, H. Ruan, Z. Sun, X. Xu, J. Yang, G. Ma, Supramolecular assemblies based on natural small molecules: union would be effective, Mater. Today Bio. 15 (2022).

[32] O.Y. Selyutina, N.E. Polyakov, Glycyrrhizic acid as a multifunctional drug carrier - from physicochemical properties to biomedical applications: a modern insight on the ancient drug, Int. J. Pharm. 559 (2019) 271–279.

[33] T. Deng, D. Gao, X. Song, Z. Zhou, L. Zhou, M. Tao, Z. Jiang, L. Yang, L. Luo, A. Zhou, L. Hu, H. Qin, M. Wu, A natural biological adhesive from snail mucus for wound repair, Nat. Commun. 14 (1) (2023) 396.

[34] J. Ouyang, Q. Bu, N. Tao, M. Chen, H. Liu, J. Zhou, J. Liu, B. Deng, N. Kong, X. Zhang, T. Chen, Y. Cao, W. Tao, A facile and general method for synthesis of antibiotic-free protein-based hydrogel: wound dressing for the eradication of drug-resistant bacteria and biofilms, Bioact. Mater. 18 (2022) 446–458.

[35] H. Xu, T. Wang, C. Yang, X. Li, G. Liu, Z. Yang, P.K. Singh, S. Krishnan, D. Ding, Supramolecular nanofibers of curcumin for highly amplified radiosensitization of colorectal cancers to ionizing radiation, Adv. Funct. Mater. 28 (14) (2018).

[36] H. Jang, K. Zhi, J. Wang, H. Zhao, B. Li, X. Yang, Enhanced therapeutic effect of paclitaxel with a natural polysaccharide carrier for local injection in breast cancer, Int. J. Biol. Macromol. 148 (2020) 163–172.

[37] Q. Liu, C. Zhan, A. Barhoumi, W. Wang, C. Santamaria, J.B. McAlvin, D.S. Kohane, A supramolecular shear-thinning anti-inflammatory steroid hydrogel, Adv. Mater. 28 (31) (2016) 6680–6686.

[38] H. Zhang, K. Liu, Y. Gong, W. Zhu, J. Zhu, F. Pan, Y. Chao, Z. Xiao, Y. Liu, X. Wang, Z. Liu, Y. Yang, Q. Chen, Vitamin C supramolecular hydrogel for enhanced cancer immunotherapy, Biomaterials 287 (2022), 121673.

[39] H. Huang, W. Gong, X. Wang, W. He, Y. Hou, J. Hu, Self-assembly of naturally small molecules into supramolecular fibrillar networks for wound healing, Adv. Healthc. Mater. 11 (12) (2022), e2102476.

[40] S.K. Dash, S. Chattopadhyay, S.S. Dash, S. Tripathy, B. Das, S.K. Mahapatra, B. G. Bag, P. Karmakar, S. Roy, Self assembled nano fibers of betulinic acid: a selective inducer for ROS/TNF-alpha pathway mediated leukemic cell death, Bioorg. Chem. 63 (2015) 85–100.

[41] G.F. Picheth, C.L. Pirich, M.R. Sierakowski, M.A. Woehl, C.N. Sakakibara, C.F. de Souza, A.A. Martin, R. da Silva, R.A. de Freitas, Bacterial cellulose in biomedical applications: a review, Int. J. Biol. Macromol. 104 (Pt A) (2017) 97–106.

[42] L. Zou, Q. Li, Y. Hou, M. Chen, X. Xu, H. Wu, Z. Sun, G. Ma, Self-assembled glycyrrhetinic acid derivatives for functional applications: a review, Food Funct. (2022).

[43] A. Kowalska, U. Kalinowska-Lis, 18beta-Glycyrrhetinic acid: its core biological properties and dermatological applications, Int. J. Cosmet. Sci. 41 (4) (2019) 325–331.

[44] A.V. Markov, A.V. Sen'kova, M.A. Zenkova, E.B. Logashenko, Novel glycyrrhetinic acid derivative soloxolone methyl inhibits the inflammatory response and tumor growth in vivo, Mol. Biol. 52 (2) (2018) 262–268.

[45] N. Liu, G.X. Zhang, Y.T. Niu, Q. Wang, J. Zheng, J.M. Yang, T. Sun, J.G. Niu, J. Q. Yu, Anti-inflammatory and analgesic activities of indigo through regulating the IKKbeta/IkappaB/NF-kappaB pathway in mice, Food Funct. 11 (10) (2020) 8537–8546.

[46] Y. Yang, Q. Zhu, Y. Zhong, X. Cui, Z. Jiang, P. Wu, X. Zheng, K. Zhang, S. Zhao, Synthesis, anti-microbial and anti-inflammatory activities of 18beta-glycyrrhetinic acid derivatives, Bioorg. Chem. 101 (2020), 103985.

[47] L.A. Stecanella, A.P.R. Bitencourt, G.R. Vaz, E. Quarta, J.O.C. Silva Junior, A. Rossi, Glycyrrhizic acid and its hydrolyzed metabolite 18beta-glycyrrhetinic acid as specific ligands for targeting nanosystems in the treatment of liver cancer, Pharm. 13 (11) (2021).

[48] B.G. Bag, R. Majumdar, Self-assembly of a renewable nano-sized triterpenoid 18β-glycyrrhetinic acid, RSC Adv. 2 (23) (2012) 8623–8626.

[49] J. Wu, J. Lu, J. Hu, Y. Gao, Q. Ma, Y. Ju, Self-assembly of sodium glycyrrhetinate into a hydrogel: characterisation and properties, RSC Adv. 3 (47) (2013) 24906–24909.

[50] L.A. Stecanella, A.P.R. Bitencourt, G.R. Vaz, E. Quarta, J.O.C. Silva Júnior, A. Rossi, Glycyrrhizic acid and its hydrolyzed metabolite 18β-glycyrrhetinic acid as specific ligands for targeting nanosystems in the treatment of liver cancer, Pharm. 13 (11) (2021) 1792.

[51] T. Li, P. Wang, W. Guo, X. Huang, X. Tian, G. Wu, B. Xu, F. Li, C. Yan, X.J. Liang, H. Lei, Natural berberine-based Chinese herb medicine assembled nanostructures with modified antibacterial application, ACS Nano 13 (6) (2019) 6770–6781.

[52] Y. Ma, Y. Gao, K. Zhao, H. Zhang, Z. Li, F. Du, J. Hu, Simple, effective, and ecofriendly strategy to inhibit droplet bouncing on hydrophobic weed leaves, ACS Appl. Mater. Interfaces 12 (44) (2020) 50126–50134.

[53] P.P. Shu, L.X. Li, Q.M. He, J. Pan, X.L. Li, M. Zhu, Y. Yang, Y. Qu, Identification and quantification of oleanane triterpenoid saponins and potential analgesic and anti-inflammatory activities from the roots and rhizomes of Panax stipuleanatus, J. Ginseng. Res. 45 (2) (2021) 305–315.

[54] Z. Li, L. Zhang, Z. Zhao, Malyngamide F possesses anti-inflammatory and antinociceptive activity in rat models of inflammation, Pain Res. Manag. 2021 (2021), 4919391.

[55] Q. Li, Z. Wan, X. Yang, Glycyrrhizic acid: self-assembly and applications in multiphase food systems, Curr. Opin. Food Sci. 43 (2022) 107–113.

[56] Y. Qian, Y. Zheng, J. Jin, X. Wu, K. Xu, M. Dai, Q. Niu, H. Zheng, X. He, J. Shen, Immunoregulation in diabetic wound repair with a photo-enhanced glycyrrhizic acid hydrogel scaffold, Adv. Mater. 34 (2022), 2200521.

[57] S. Guo, S. Chen, N. Cao, W. Zheng, D. Li, Z. Sheng, X. Xu, Q. Zhang, X. Zheng, K. Wu, P. Wu, K. Zhang, W.D. Hong, A novel 18β-glycyrrhetinic acid derivative supramolecular self-assembly hydrogel with antibacterial activity, J. Mater. Sci. 56 (30) (2021) 17254–17267.

[58] J.P. Fan, H. Zhong, X.H. Zhang, T.T. Yuan, H.P. Chen, H.L. Peng, Preparation and characterization of oleanolic acid-based low-molecular-weight supramolecular hydrogels induced by heating, ACS Appl. Mater. Interfaces 13 (24) (2021) 29130–29136.

[59] Y. Hou, M. Chen, H. Ruan, Z. Sun, H. Wu, X. Xu, J. Yang, G. Ma, X. Zhou, A new supramolecular natural product gel based on self-assembled pomolic acid from traditional Chinese medicine, Colloid and Interface Sci. Commun. 46 (2022).

[60] Q. Chen, C. Wang, X. Zhang, G. Chen, Q. Hu, H. Li, J. Wang, D. Wen, Y. Zhang, Y. Lu, G. Yang, C. Jiang, J. Wang, G. Dotti, Z. Gu, In situ sprayed bioresponsive immunotherapeutic gel for post-surgical cancer treatment, Nat. Nanotechnol. 14 (1) (2018) 89–97.

[61] J. Ouyang, X. Ji, X. Zhang, C. Feng, Z. Tang, N. Kong, A. Xie, J. Wang, X. Sui, L. Deng, Y. Liu, J.S. Kim, Y. Cao, W. Tao, In situ sprayed NIR-responsive, analgesic black phosphorus-based gel for diabetic ulcer treatment, Proc. Natl. Acad. Sci. U. S. A. 117 (46) (2020) 28667–28677.

[62] M. Munoz, C. Eren Cimenci, K. Goel, M. Comtois-Bona, M. Hossain, C. McTiernan, M. Zuniga-Bustos, A. Ross, B. Truong, D.R. Davis, W. Liang, B. Rotstein, M. Ruel, H. Poblete, E.J. Suuronen, E.I. Alarcon, Nanoengineered sprayable therapy for treating myocardial infarction, ACS Nano 16 (3) (2022) 3522–3537.

[63] R.J.A. Moakes, S.P. Davies, Z. Stamataki, L.M. Grover, Formulation of a composite nasal spray enabling enhanced surface coverage and prophylaxis of SARS-COV-2, Adv. Mater. 33 (26) (2021), e2008304.

[64] S. Ma, Z. Cong, J. Wei, W. Chen, D. Ge, F. Yang, Y. Liao, Pulmonary delivery of size-transformable nanoparticles improves tumor accumulation and penetration for chemo-sonodynamic combination therapy, J. Contr. Release 350 (2022) 132–145.

[65] Y. Yang, J. Yuan, Y. Ni, Y. Gu, J. Zhou, W. Yuan, S. Xu, L. Che, S.Y. Zheng, W. Sun, D. Zhang, J. Yang, Spatiotemporal self-strengthening hydrogels for oral tissue regeneration, Composites Part B, Engineering 243 (2022).

[66] X. Du, J. Zhou, J. Shi, B. Xu, Supramolecular hydrogelators and hydrogels: from soft matter to molecular biomaterials, Chem. Rev. 115 (24) (2015) 13165–13307.

[67] Y. Zou, P. Yue, H. Cao, L. Wu, L. Xu, Z. Liu, S. Wu, Q. Ye, Biocompatible and biodegradable chitin-based hydrogels crosslinked by BDDE with excellent mechanical properties for effective prevention of postoperative peritoneal adhesion, Carbohydr. Polym. 305 (2023).

[68] L. Jiang, F. Yao, E. Zhang, Q. Yu, C. Yu, Z. Chen, J. Chen, Z. Yue, P. Che, J. Li, H. Sun, Combined treatment of xyloglucan derivative hydrogel and anti-C5a receptor antibody in preventing peritoneal adhesion, Acta Biomater. 151 (2022) 163–173.

[69] S.P. Carmichael, J. Shin, J.W. Vaughan, P.K. Chandra, J.B. Holcomb, A.J. Atala, Regenerative medicine therapies for prevention of abdominal adhesions: a scoping review, J. Surg. Res. 275 (2022) 252–264.

[70] X. Zhao, H. Zhang, Y. Gao, Y. Lin, J. Hu, A simple injectable moldable hydrogel assembled from natural glycyrrhizic acid with inherent antibacterial activity, ACS Appl. Bio Mater. 3 (1) (2020) 648–653.

[71] K. Oyama, M. Kawada-Matsuo, Y. Oogai, T. Hayashi, N. Nakamura, H. Komatsuzawa, Antibacterial effects of glycyrrhetinic acid and its derivatives on Staphylococcus aureus, PLoS One 11 (11) (2016), e0165831.

[72] H.K. Kim, Y. Park, H.N. Kim, B.H. Choi, H.G. Jeong, D.G. Lee, K.-S. Hahm, Antimicrobial mechanism of β-glycyrrhetinic acid isolated from licorice, Glycyrrhiza glabra, Biotechnol. Lett. 24 (22) (2002) 1899–1902.

[73] H. Wu, Y. Wang, Y. Zhang, F. Xu, J. Chen, L. Duan, T. Zhang, J. Wang, F. Zhang, Breaking the vicious loop between inflammation, oxidative stress and coagulation, a novel anti-thrombus insight of nattokinase by inhibiting LPS-induced inflammation and oxidative stress, Redox Biol. 32 (2020).

[74] J. Ouyang, B. Deng, B. Zou, Y. Li, Q. Bu, Y. Tian, M. Chen, W. Chen, N. Kong, T. Chen, W. Tao, Oral hydrogel microbeads-mediated in situ synthesis of selenoproteins for regulating intestinal immunity and microbiota, J. Am. Chem. Soc. 145 (22) (2023) 12193–12205.

[75] X. Peng, X. Xia, X. Xu, X. Yang, B. Yang, P. Zhao, W. Yuan, P.W.Y. Chiu, L. Bian, Ultrafast self-gelling powder mediates robust wet adhesion to promote healing of gastrointestinal perforations, Sci. Adv. 7 (23) (2021), eabe8739.

[76] T. Deng, D. Gao, X. Song, Z. Zhou, L. Zhou, M. Tao, Z. Jiang, L. Yang, L. Luo, A. Zhou, L. Hu, H. Qin, M. Wu, A natural biological adhesive from snail mucus for wound repair, Nat. Commun. 14 (1) (2023) 396.